J. Phys. Chem. A **2007,** *111,* 4737−4742

Photoactivity and UV Absorption Spectroscopy of $RCo(CO)_4$ ($R = H, CH_3$) Organometallic Complexes

David Ambrosek,[†] Sebastien Villaume,[‡] Chantal Daniel,*[,‡] and Leticia González*[,†]

Institut für Chemie und Biochemie, Freie Universität Berlin, Takustrasse 3, 14195 Berlin, Germany, and Institut de Chimie, Laboratoire de Chimie Quantique, UMR 7177 CNRS/ULP 4 Rue Blaise Pascal, 67000 Strasbourg, France

Received: January 18, 2007; In Final Form: March 16, 2007

The photoactivity of $RCo(CO)_4$ ($R = H, CH_3$) complexes has been investigated and compared by means of state correlation diagrams connecting the low-lying singlet ^1E ($d_{Co} \rightarrow \sigma^*_{Co-R}$ and $d_{Co} \rightarrow \pi^*_{CO}$) and $^1A_1$ ($d_{Co} \rightarrow \pi^*_{CO}$) electronic states accessible through UV irradiation, and the low-lying triplet states (^3E and $^3A_1$), to the corresponding states of the primary products $R + Co(CO)_4$ and $CO_{ax} + RCo(CO)_3$. The electronic absorption spectra have been calculated by time-dependent wave packet propagations on two-dimensional potential energy surfaces describing both channels of dissociation, namely the homolysis of the R−Co and the CO_{ax}−Co bonds. It is shown that the absorption spectrum of $HCo(CO)_4$ is characterized by two peaks; the most intense peaks for each set are located respectively at 42 659 and 45 001 cm^{-1}. The $CH_3Co(CO)_4$ absorption spectrum also gives two sets of signals with maximum intensities found at 42 581 and 51 515 cm^{-1} These bands for both molecules are assigned to the two metal-to-ligand-charge-transfer (MLCT; $d_{Co} \rightarrow \pi^*_{CO}$) states. Three photoactive states have been determined in both molecules, namely the singlet metal-to-σ-bond-charge-transfer (MSBCT) states (a^1E and b^1E), simultaneously dissociative for both the homolysis of CO and the R−Co bond, and the $^3A_1$ ($\sigma_{Co-R} \rightarrow \sigma^*_{Co-R}$), dissociative along the R−Co bond.

1. Introduction

Ultrafast dissociation of a carbonyl ligand is the most common primary reaction observed when ultraviolet (UV) light irradiates transition metal carbonyls. In most cases this primary reaction competes with the homolysis of a metal−metal bond ($Mn_2(CO)_{10}$),[1] metal−alkyl bond ($RMn(CO)_3$(α-diimine), R = methyl, ethyl, benzyl),[2] metal−methyl bond ($MeMn(CO)_5$,[3] $MeCo(CO)_4$),[4] or metal−hydrogen bond ($HCo(CO)_4$, $HMn(CO)_5$).[5,6] Despite the number of experimental and theoretical studies devoted to this class of compounds, the knowledge of their electronic spectroscopy and photoreactivity is still limited. The ground state properties and reactivity of $RCo(CO)_4$ and $RMn(CO)_5$ ($R = H, CH_3$) have been extensively studied by means of Density Functional Theory (DFT)[7−8] while the electronic spectroscopy, photochemistry, and quantum dynamics of $HCo(CO)_4$ and $HMn(CO)_5$ have been investigated by accurate ab initio methods supplemented by wave packet dynamics.[9−11]

In a recent detailed study of the electronic excited states of $RCo(CO)_4$ ($R = H, CH_3$) by means of multistate complete active space second order perturbation theory (MS-CASPT2) and time-dependent density functional theory (TD−DFT), we have shown that the UV energy domain for the absorption spectra of both complexes is dominated by a series of allowed low-lying ^1E metal-to-σ-bond-charge-transfer (MSBCT) and ^1E and $^1A_1$ metal-to-ligand-charge-transfer (MLCT) transitions, which are slightly red-shifted (by ca. 1800 cm^{-1}) in the methyl substituted complex.[12]

The aim of the present work is to obtain the main features of the UV absorption spectra of $RCo(CO)_4$ ($R = H, CH_3$) by time-dependent wave packets propagated on two-dimensional potential energy surfaces (PES) associated with the four low-lying a^1E, b^1E MSBCT and c^1E, b^1A_1 MLCT excited states. Furthermore, we aim to determine the photoactive electronic excited states for the homolysis of the metal-hydrogen and metal-alkyl bonds and for that of the axial carbonyl. Another goal of the present theoretical study is to check the potential of these two transition metal carbonyl hydrides as good candidates for laser control of ultrafast (below one picosecond) photofragmentation into concurrent primary products. The novelty of this article regarding previous contributions is to provide a comparative study, based on state correlation diagrams and wave packet propagations, of the photoactivity and UV spectroscopy of $CH_3Co(CO)_4$ and $HCo(CO)_4$. Moreover, the detailed theoretical studies reported until now on $HCo(CO)_4$[9,10] focused only on two electronic states, namely the a^1E (MSBCT) and a^3A_1 ($\sigma_{Co-H} \rightarrow \sigma^*_{Co-H}$) states.

2. Computational details

2.1. Ab Initio Quantum Chemistry. The quantum chemical calculations for the $RCo(CO)_4$ organometallic complexes have been performed under C_s symmetry keeping the C_{3V} symmetry constraints. For $HCo(CO)_4$, both the optimized DFT(B3LYP)[12] and experimental structures[13] were employed, whereas for $CH_3Co(CO)_4$ the geometry was taken from ref 12, optimized within C_s symmetry at the DFT (B3LYP) level of theory. The structures were optimized only for the $^1A_1$ electronic ground state closed shell configuration. As shown in Figure 1, both complexes show a distorted bipyramidal trigonal structure, where one CO and $R = H, CH_3$ are in axial positions, while the other three carbonyl groups are in equatorial positions.

The electronic configuration of $RCo(CO)_4$ ($R = H, CH_3$) in its $^1A_1$ ground state is described by $(\sigma_{Co-R})^2 (3d_\pi)^4 (3d_\delta)^4$, where

---

* To whom correspondence should be addressed. E-mails: leti@chemie.fu-berlin.de (L.G.), daniel@quantix.u-strasbg.fr (C.D.).

[†] Freie Universität Berlin.

[‡] Laboratoire de Chimie Quantique.

10.1021/jp0704259 CCC: \$37.00

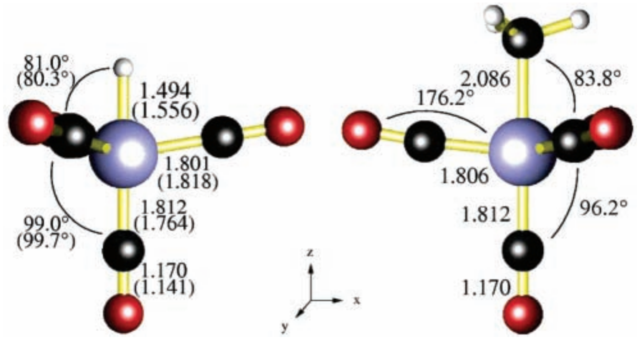

Figure 1. Schematic representation of $HCo(CO)_4$ (a) and $CH_3Co(CO)_4$, (b) with the molecular axis assumed in this work. Most important geometrical parameters are given, distances in Å and angles in deg, adapted from ref 12.

the bonding σ_{Co-R} orbital has a_1 symmetry, and the $3d_\pi$ and $3d_\delta$ orbitals belong to e symmetry. The low-lying vacant orbitals correspond to the σ^*_{Co-R} and π^*_{CO} antibonding orbitals. More details can be found in ref 12. All the calculations have been performed using the multiconfigurational complete active space SCF (CASSCF) method[14] and multistate Complete Active Space second Order Perturbation (MS-CASPT2)[15] with the MOLCAS 6.0 package.[16] The CASSCF correlation diagrams have been calculated in both complexes using an active space of 10 electrons correlated in 14 active orbitals CAS(10,14) by means of state-averaged approach including 9(A′) and 8(A″) states (the electronic ground state of A' symmetry and eight excited states) of $HCo(CO)_4$ and 5(A′) and 4(A″) states (the electronic ground state of A' symmetry and four excited states) of $CH_3Co(CO)_4$. The asymptotic limits are obtained with the corresponding R or CO_{ax} ligands at 50 Å while the rest of the geometry is kept frozen at the equilibrium. A level shift of 0.3 au has been used in the MS-CASPT2 calculations to get rid of the dramatic problem of intruder states. The same nonrelaxed approach is followed in order to calculate the PES at the CASSCF level along the internuclear coordinates, q_1 and q_2, defined as the distances d(Co−R) and d(Co−CO_{ax}), respectively. This approach is justified in that the direct dissociation of the ligands R and CO will typically take place in less than 100 femtoseconds (fs). Obviously, other relaxation effects such as the umbrella motion of the three equatorial carbonyls or the stretching of the carbonyls could be investigated in a more advanced study. The relevant PES have been calculated using a CAS (10,14) and CAS (10,12) for R = H, CH_3 complexes, respectively, and the same number of roots as specified above. Note that in this case, only the A' symmetry has been considered. The potential functions used in the wave packet propagations were constructed by a spline fit technique over ~150 ab initio points.

The following atomic natural orbital (ANO-Small) basis sets[17] are employed for both complexes: a (17s, 12p, 9d, 4f) contracted to [6s, 4p, 3d, 2f] for the cobalt atom, a (10s, 6p, 3d) contracted to [3s, 2p, 1d] for the C and O atoms and a (7s, 3p) contracted to [2s, 1p] for the hydrogen atom. Because we are working in C_s symmetry, a subgroup of C_{3v}, the ^1E states are described as degenerate states from $^1A'$ and $^1A''$ symmetries, which have been then paired by averaging the excitation energies. In both complexes a set of five roots averaged for the A' symmetry and four averaged states for the A'' symmetry have been used in the singlet and triplet CASSCF calculations.

2.2. Time-Dependent UV Absorption Spectrum. Following Heller[18] the UV absorption spectrum can be calculated using a time-dependent approach. For this purpose we solve the time-dependent Schrödinger equation

$$\left[i\hbar\frac{\partial}{\partial t} - \hat{H}_{ij}(q_1,q_2)\right]\Phi_i(q_1,q_2;t) = 0 \qquad (1)$$

where $\hat{H}_{ij}$ is the total Hamiltonian composed of the kinetic operator $\hat{T}$ and the potential operator, given by the adiabatic PES, $\hat{V}_i(q_1,q_2)$, on which the time-dependent nuclear wave packets $\Phi_i(q_1,q_2;t)$ are propagated.

The kinetic energy operator, defining the dissociation of the CO and the H or CH_3 ligands, in a reduced 2-D model (Scheme 1), is given by

$$\hat{T} = -\frac{\hbar^2}{2m_1}\frac{\partial^2}{\partial {q_1}^2} - \frac{\hbar^2}{2m_2}\frac{\partial^2}{\partial {q_2}^2} + \frac{\hbar^2}{m_{Co(CO)3}}\frac{\partial}{\partial q_1}\frac{\partial}{\partial q_2} \qquad (2)$$

with reduced masses of

$$m_1 = \frac{m_R \cdot m_{Co(CO)3}}{m_R + m_{Co(CO)3}} \quad \text{and} \quad m_2 = \frac{m_{CO} \cdot m_{Co(CO)3}}{m_{CO} + m_{Co(CO)3}} \qquad (3)$$

where R = H, CH_3. Accordingly, $m_1 = 0.99$ and 13.58 amu, for $HCo(CO)_4$ and $CH_3Co(CO)_4$, respectively, and $m_2 = 23.41$ amu. The absorption spectrum is then calculated as the Fourier transformation of the time-dependent total autocorrelation function, $S_{tot}(t)$:

$$\sigma(\omega) \propto \int_{-\infty}^{+\infty} dt\, S_{tot}(t) \cdot \exp(i(E_{00} + \hbar\omega)t/\hbar) \qquad (4)$$

where E_{00} is the energy of the vibrational ground state of the electronic ground state, and $\hbar\omega$ is the energy of the absorbed photon. The total autocorrelation function is the sum over the individual autocorrelation functions corresponding to each electronically excited state j:

$$S_{tot}(t) = \sum_j S_j(t) = \sum_j \langle \Phi_j(q_1,q_2;t=0) | \Phi_j(q_1,q_2;t) \rangle \qquad (5)$$

and describes the evolution of the molecular system on all of the electronically excited states by tracking the overlap of the wave function $\Phi_j(t)$ with the initial wave function $\Phi_j(t = 0)$ as a function of time t. The initial wave function is calculated as

$$\Phi_j(q_1,q_2;t=0) = \tilde{\mu}_{ji} \cdot \phi_{00}(q_1,q_2) \qquad (6)$$

that is, we demand that the initial wave packet in the upper electronic state j equals the wave function of the vibrational ground state $\phi_{00}(q_1,q_2)$ multiplied by the normalized transition dipole moments $\tilde{\mu}_{ji}$ at the Franck−Condon point, defined as

$$\tilde{\mu}_{ji} \equiv \tilde{\mu}_{j0} = \frac{\sqrt{{\mu_{j0,x}}^2 + {\mu_{j0,y}}^2 + {\mu_{j0,z}}^2}}{\sum_j \mu_{j0}} \qquad (7)$$

The vibrational eigenstate $\phi_{00}(q_1,q_2)$ is calculated using the Fourier Grid Hamiltonian method,[19] with a spatial discretization of 64 × 64 = 4096 grid points. The time-dependent propagation of the wave function is carried out on a larger grid of 256 × 256 = 65 536 for the methyl complex and 128 × 1024 = 131 072 grid points for the hydrido complex, as indicated in Table 1, using the split-operator method,[20] as implemented in the Wavepacket set of programs,[21] with a time step of 0.01 fs during 1 ps. The respective spatial grids employed in the calculation of the eigenfunctions and in the time-dependent propagations for both complexes are collected in Table 1. In order to avoid unphysical reflections of the wave functions, an absorbing

SCHEME 1

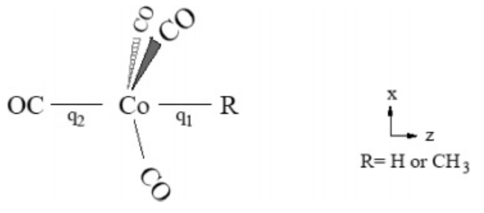

TABLE 1: Regular Spatial Grids Employed for the Calculation of the Initial Eigenfunction ϕ_{00} and for the Propagation of the Wave Function $\Phi_i(t)$ in the 2-D PES of HCo(CO)$_4$ and CH$_3$Co(CO)$_4$[a]

	Eigenfunction	propagation
	HCo(CO)$_4$	
$q_1 = d$(Co−R)	1.0−2.47 Å (64 points)	1.0−24.52 Å (1024 points)
$q_2 = d$(Co−CO)	1.5−2.49 Å (64 points)	1.5−3.48 Å (128 points)
	CH$_3$Co(CO)$_4$	
$q_1 = d$(Co−R)	1.8−3.20 Å (64 points)	1.8−7.40 Å (256 points)
$q_2 = d$(Co−CO)	1.72−3.02 Å (64 points)	1.72−6.92 Å (256 points)

[a] The number of grid points along one dimension in each case is indicated in parenthesis.

TABLE 2: CASSCF and MS-CASPT2 Co−R (R = H, CH$_3$) and Co−CO$_{ax}$ Bond Dissociation Energies (in kcal mol^{-1}) in HCo(CO)$_4$ and CH$_3$Co(CO)$_4$ Compared to the Available Experimental Data and Other Theoretical Values

	CASSCF	MS-CASPT2	experimental[23]	other theoretical studies[24]
		HCo(CO)$_4$		
Co−H	62.2	76.6	57.0	55.0
Co−CO$_{ax}$	37.9	65.8		
		CH$_3$Co(CO)$_4$		
Co−CH$_3$	37.0	60.6		38.27
Co−CO$_{ax}$	20.0	55.2		

TABLE 3: CASSCF Relative Energies in kcal mol^{-1} at Equilibrium and Dissociation Limits of RCo(CO)$_4$ (R = H, CH$_3$)[a]

state		singlet			state		triplet		
C_{3v}	C_s	equil	CO diss	R diss	C_{3v}	C_s	equil	CO diss	R diss
				HCo(CO)$_4$					
a^{1}A$_1$	^{1}A′	0.0	37.90	62.19					
a^{1}E	^{1}A′	113.83	81.89	86.66	a^{3}E	^{3}A′	95.57	65.64	85.91
	^{1}A″	115.78	86.53	87.54		^{3}A″	92.24	64.32	86.16
b^{1}E	^{1}A′	121.42	96.89	95.76	b^{3}E	^{3}A	103.80	78.19	93.88
	^{1}A″	122.80	96.76	97.64		^{3}A″	100.78	77.56	96.51
c^{1}E	^{1}A′	130.96		179.53	c^{3}E	^{3}A′	117.28		165.85
	^{1}A″	128.45		178.71		^{3}A″	117.34		165.41
b^{1}A$_1$	^{1}A′	136.48		183.67	b^{3}A$_1$	^{3}A′	106.17		158.89
					a^{3}A$_1$	^{3}A′	138.68		61.31
				CH$_3$Co(CO)$_4$					
a^{1}A$_1$	^{1}A′	0.0	20.52	37.46					
a^{1}E	^{1}A′	104.10	63.76	62.19	a^{3}E	^{3}A′	85.72	46.31	62.37
	^{1}A″	106.93	67.21	66.64		^{3}A″	79.57	48.69	65.32
					a^{3}A$_1$	^{3}A′	88.10	78.19	38.59
b^{1}E	^{1}A′	114.96	67.33	70.59	b^{3}E	^{3}A′	94.88	50.95	70.41
	^{1}A″	115.21	72.04	74.92		^{3}A″	115.21	72.038	74.92
c^{1}E	^{1}A′	121.99			c^{3}E	^{3}A′	114.77		
	^{1}A″	121.92				^{3}A″	114.96		
b^{1}A$_1$	^{1}A′	128.20							

[a] The relative energies are calculated with respect to the equilibrium a^{1}A$_1$ ground state energy (−1833.1934 au) for HCo(CO)$_4$ and (−1872.2090 au) for CH$_3$Co(CO)$_4$, respectively.

boundary potential[22] has been established at 6.40 and 6.00 Å for the methyl complex and 23.0 and 3.3 Å for the hydrido complex along the q$_1$ and q$_2$ coordinates, respectively.

3. Results and Discussion

3.1. Bond Dissociation Energies. The bond dissociation energies of HCo(CO)$_4$ and CH$_3$Co(CO)$_4$ calculated at the CASSCF and MS-CASPT2 levels of theory are reported in Table 2 together with the experimental data when available[23] and other theoretical values.[24,25]

The calculated Co−CO$_{ax}$ bond dissociation energies may be compared to both experimental and theoretical values discussed in ref 25 for Fe(CO)$_5$, Ni(CO)$_4$ and Cr(CO)$_6$, respectively in the range 39.0−44.2, 25.0−29.8, and 32.7−42.7 kcal mol^{-1}.

While the CASSCF dissociation energies are surprisingly in reasonable agreement with the experimental and other theoretical studies, the MS-CASPT2 method fails at reproducing correctly this property for the Co−R (R = H, CH$_3$) bond as well as for the Co−CO$_{ax}$ bond with a systematic overestimation of the order of 20.0−30.0 kcal mol^{-1}. This effect is more significant for the Co−CO$_{ax}$ bond than for the Co−R (R = H, CH$_3$) bond. This is a consequence of the unbalanced description of the equilibrium and asymptotic electronic structures by means of perturbation theory using a level shift technique and based on a rather limited CASSCF zero-order wavefunction. In particular, while a correct description of the Co−R σ interaction is warranted at the equilibrium structure by the presence in the active space of the σ_{Co-R} and σ^*_{Co-R} orbitals this is not the case at the asymptote. Since this failure on the dissociation energies could be corrected only by the use of a huge active space combined with full geometry optimization of both the reactants and primary products at the same level of theory, the state correlation diagrams and the PES presented in the next section have been built at the CASSCF level. This level of calculation should be adequate to draw a qualitative picture of a direct ultrafast deactivation mechanism after UV absorption of the two complexes.

3.2. State Correlation Diagrams. The CASSCF energies of the a^{1}A$_1$ electronic ground state, a^{3}A$_1$ ($\sigma_{Co-R} \rightarrow \sigma^*_{Co-R}$), a^{1,3}E and b^{1,3}E MSBCT excited states and c^{1,3}E and b^{1,3}A$_1$ MLCT excited states calculated at the equilibrium geometry for HCo(CO)$_4$ (Figure 1a) and CH$_3$Co(CO)$_4$ (Figure 1b) and at bond distances of 50.0 Å for Co−R and Co−CO$_{ax}$ are reported in Table 3.

The corresponding state correlation diagrams for HCo(CO)$_4$ and CH$_3$Co(CO)$_4$, depicted in Figure 2 and Figure 3, respectively, present the connections between the low-lying electronic states and their corresponding states leading to the primary products R$^\bullet$ + $^\bullet$Co(CO)$_4$ or CO$_{ax}$ + RCo(CO)$_3$.

Before we discuss the state correlation diagrams based on CASSCF relative energies, the CASSCF transition energies of the low-lying singlet absorbing excited states should be compared to those obtained at the MS-CASPT2 level in ref 12 (Table 4).

The relative order of the four low-lying singlet states (a^{1}E, b^{1}E, c^{1}E, and b^{1}A$_1$) is not modified when going from the CASSCF to the MS-CASPT2 level and is qualitatively correct. The present MS-CASPT2 values differ from the previous theoretical study[12] due to different CASSCF active spaces.

The lowest a^{1}E and b^{1}E MSBCT absorbing states of HCo(CO)$_4$ calculated at 35 740 cm^{-1} and 40 280 cm^{-1} at the MS-CASPT2 level[12] are dissociative with respect to the cobalt-hydrogen bond homolysis as well as to the axial carbonyl dissociation. The upper MLCT states (c^{1}E, b^{1}A$_1$) are bound and should not participate in the UV photoreactivity of HCo(CO)$_4$.

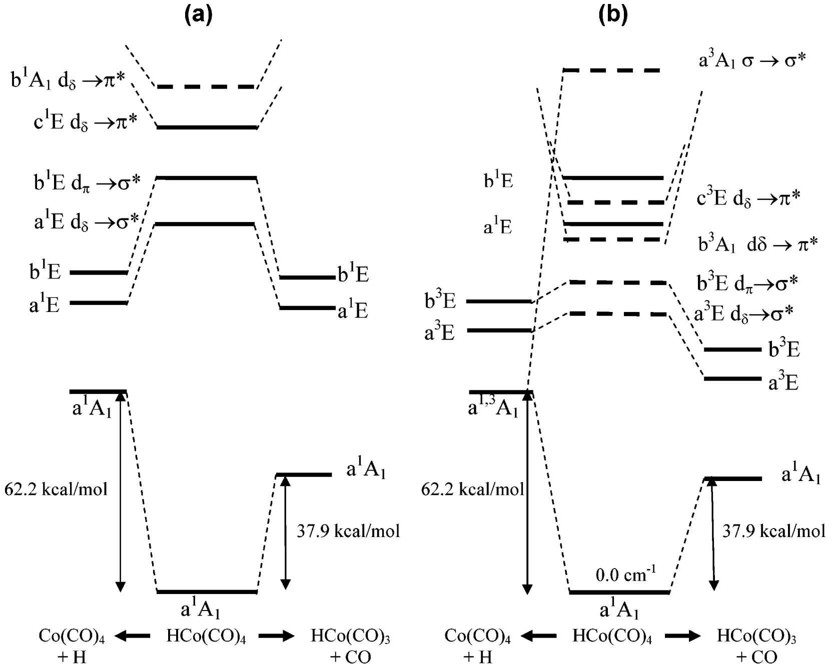

Figure 2. State correlation diagrams calculated at CASSCF level of theory for the singlet (a) and also triplet (b) states of $HCo(CO)_4$ for 9A′ and 8A″ roots (see text).

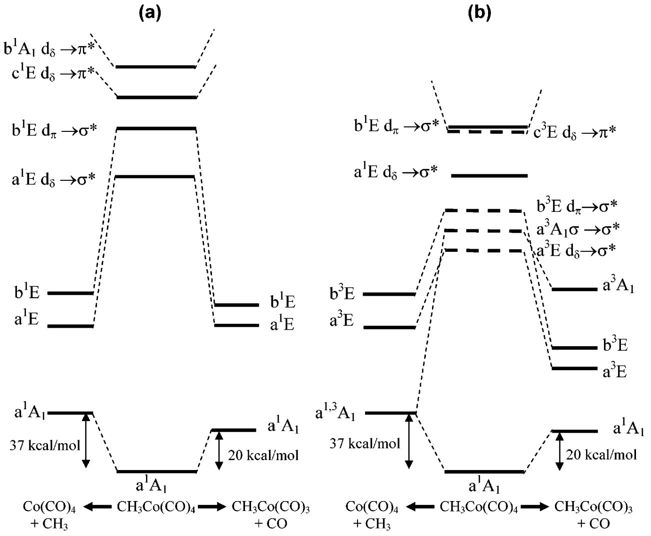

Figure 3. State correlation diagrams calculated at CASSCF level of theory for the singlet (a) and also triplet (b) states of $CH_3Co(CO)_4$ for 5A′ and 4A″ roots (see text).

TABLE 4: CASSCF and MS-CASPT2 Transition Energies (in cm^{-1}) to the Low-Lying Singlet Absorbing States of $HCo(CO)_4$ and $CH_3Co(CO)_4$

state	main configuration	CASSCF(10,14)	MS-CASPT2[a]
	$HCo(CO)_4$		
$a^1A_1 \rightarrow a^1E$	$3d_{Co} \rightarrow \sigma^*_{Co-H}$	40 150	35 740
$a^1A_1 \rightarrow b^1E$	$3d_{Co} \rightarrow \sigma^*_{Co-H}$	42 710	40 280
$a^1A_1 \rightarrow c^1E$	$3d_{Co} \rightarrow \pi^*_{CO}$	45 360	41 320
$a^1A_1 \rightarrow b^1A_1$	$3d_{Co} \rightarrow \pi^*_{CO}$	47 730	42 040
	$CH_3Co(CO)_4$		
$a^1A_1 \rightarrow a^1E$	$3d_{Co} \rightarrow \sigma^*_{Co-Me}$	36 910 (37230)[b]	33 980
$a^1A_1 \rightarrow b^1E$	$3d_{Co} \rightarrow \sigma^*_{Co-Me}$	40 250 (39000)[b]	38 390
$a^1A_1 \rightarrow c^1E$	$3d_{Co} \rightarrow \pi^*_{CO}$	42 660 (43670)[b]	40 720
$a^1A_1 \rightarrow b^1A_1$	$3d_{Co} \rightarrow \pi^*_{CO}$	44 840 (54870)[b]	42 340

[a] Taken from ref 12. [b] Values in parenthesis correspond to CASSCF(10,12) and *A*′ symmetry.

The photofragmentation of the molecule in gas phase, according to a direct and ultrafast mechanism, into H$^•$ + $^•$Co(CO)$_4$ and CO + $HCo(CO)_3$ primary products within a few hundred femtoseconds after UV irradiation, is highly probable. When the triplet states are taken into account (Figure 2b) the photodissociation may occur via intersystem crossing from the a,b^1E absorbing states to the low-lying a^3E, b^3E, and $^3A_1$ states, all of which are dissociative. In particular, the a^3A_1 ($\sigma_{Co-H} \rightarrow \sigma^*_{Co-H}$) state will lead to the H$^•$ + $^•$Co(CO)$_4$ ($^{1,3}A_1$) diradical primary products according to the mechanism proposed in our previous work.[10] This mechanism, alternative to a direct ultrafast deactivation via the singlet absorbing states will occur within a picosecond time-scale.

The lowest a^1E and b^1E MSBCT absorbing states of $CH_3Co(CO)_4$ calculated at 33 980 cm^{-1} and 38 390 cm^{-1} at the MS-CASPT2 level[12] are clearly dissociative for both channels, namely the Co−CH_3 bond homolysis and the CO loss. The upper c^1E and b^1A_1 MLCT states are bound and no correlation was found with the low-lying states of the primary products at dissociation. The mechanism of ultrafast gas-phase photofragmentation based on the low-lying singlet states is similar to the one proposed for $HCo(CO)_4$ leading to $^•CH_3$ + $^•$Co(CO)$_4$ and CO + $CH_3Co(CO)_3$ fragments within a few hundred femtoseconds. Again the a^3A_1 ($\sigma_{Co-CH3} \rightarrow \sigma^*_{Co-CH3}$) will play a key role in the formation of the diradical primary products within picoseconds after intersystem crossing. However, these effects could be investigated in a further study devoted to the determination of dissociation time scales and branching ratio.

3.3. Two-Dimensional Potential Energy Surfaces and Photoactivity. In order to investigate in more detail the mechanism of ultrafast photodissociation of both molecules the 2-D adiabatic potential energy surfaces have been built as a function of the metal−R (q_1) and metal−CO$_{ax}$ (q_2) bond distances for the a^1A_1 electronic ground state and the four low-lying MSBCT (a^1E and b^1E) and MLCT states (c^1E and b^1A_1). The 1-D cuts along q_1 and q_2 are shown in Figure 4.

As predicted from the state-correlation diagrams shown in Figures 2 and 3, the lowest two MSBCT (a^1E and b^1E) states are strongly repulsive along both dissociation channels. At the Frank-Condon (FC) region the gradients are steeper along the Co−R bond coordinate, and therefore dissociation of H or CH_3 is faster than Co−CO. This is confirmed by propagating the

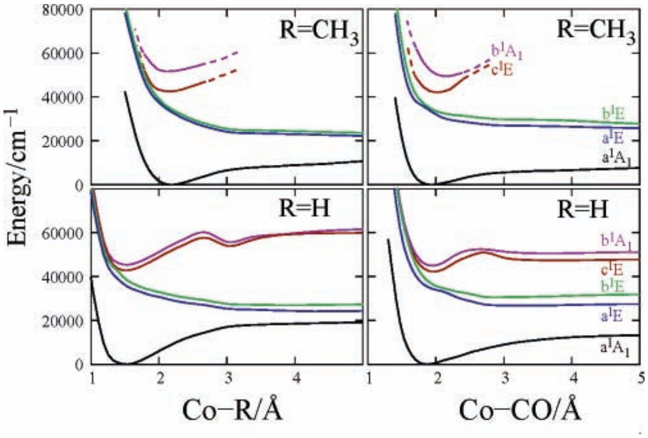

Figure 4. One-dimensional potential energy cuts along q_1(Co−R) and q_2(Co−CO) coordinates for RCo(CO)$_4$.

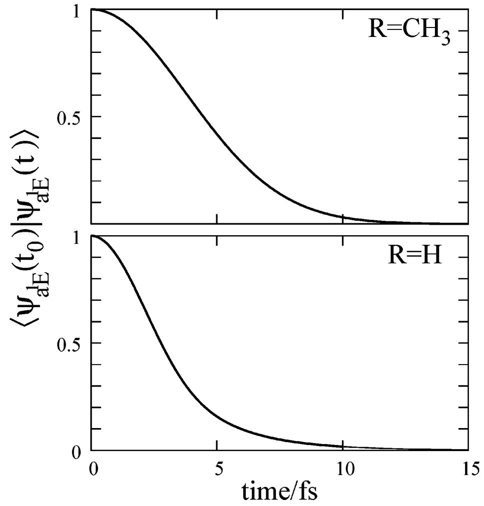

Figure 5. Autocorrelation functions in the a^{1}E state of HCo(CO)$_4$ (a) and CH$_3$Co(CO)$_4$ (b).

initial vibrational ground state wave function on any of the MSBCT surfaces, and watching the autocorrelation function, which is an indicator of the rate at which dissociation occurs. Exemplarily, the autocorrelation functions $S_j(t)$ on the repulsive a^{1}E state are shown in Figure 5.

For HCo(CO)$_4$, dissociation occurs along the H channel and $S_{a^1E}(t)$ reaches the reciprocal of e after 3.4 fs. In CH$_3$Co(CO)$_4$, the same value is reached after 5.3 fs and both the CO and CH$_3$ are fragmented.

According to the bounded shape of the upper MLCT states (c^{1}E and b^{1}A$_1$), the system will be trapped in their corresponding potential wells when these states are populated, and energy will be redistributed among other vibrational modes. The minima in the MLCT states are located at q_1 = 1.552, q_2 = 1.999 Å and q_1 = 1.552, q_2 = 1.905 Å for HCo(CO)$_4$ and q_1 = 2.195, q_2 = 2.026 Å and q_1= 2.195, q_2 = 2.169 Å, for CH$_3$Co(CO)$_4$, for the c^{1}E and b^{1}A$_1$ states respectively. These MLCT states are also characterized by several avoided crossings before 3 Å, more clearly depicted in the case of HCo(CO)$_4$ for which the c^{1}E,b^{1}A$_1$ states have been computed until dissociation. Because these potential crossings appear at distances much larger than the minima, and a vertical excitation has not enough kinetic energy to overcome the respective barrier, the system will not explore this region of the adiabatic PESs and therefore, nonadiabatic couplings do not need to be taken into account within the limit of a short time-scale simulation.

3.4. Time-Dependent Absorption Spectrum. The normalized absorption spectra for RCo(CO)$_4$ simulated through time-dependent wave packet propagations on adiabatic 2-D surfaces are shown in Figure 6. For both complexes, the spectrum is characterized by two main bands, which correspond to the bound c^{1}E and b^{1}A$_1$ MLCT states, with respective vibrational progressions for the metal−ligand stretching modes. As expected, the position of the bands agrees with the CASSCF values listed in Table 4.

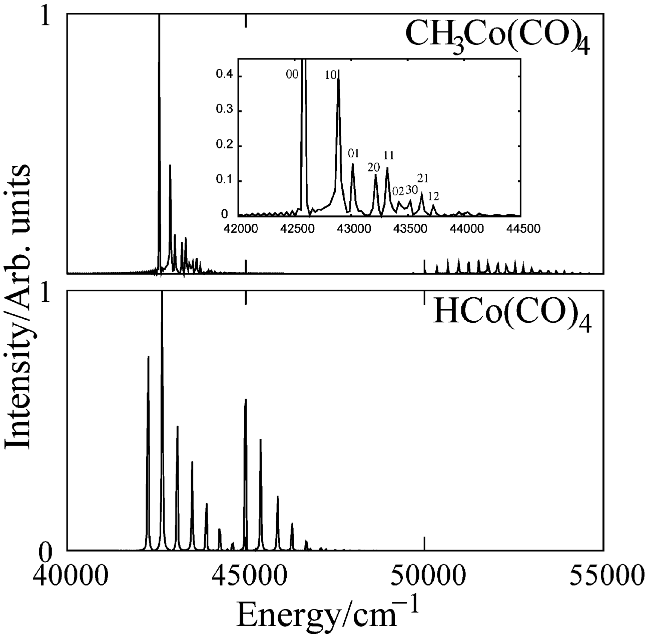

Figure 6. Normalized theoretical absorption spectra for RCo(CO)$_4$ complexes. The inset shows the vibrational progression between 42 000 and 44 500 cm^{-1} of the c^{1}E electronic state (the labels correspond to the vibrational eigenstates $\phi_{nm}(q_1,q_2)$ where n and m indicate the number of nodes in q_1 and q_2 coordinates, respectively).

For HCo(CO)$_4$ (bottom of Figure 6), the first band corresponds to the c^{1}E state and stretches from 42 280 to 44 700 cm^{-1}; the second band corresponds to the b^{1}A$_1$ state and extends from 45 000 to 47 100 cm^{-1}. The absorption spectrum of HCo(CO)$_4$ is not directly comparable to the experimental absorption spectrum recorded in an argon matrix[5] which is characterized by an intense band between 36 000 and 43 480 cm^{-1}. The maximum peaks of the calculated spectrum are observed at 42 660 and 45 000 cm^{-1} for the c^{1}E and b^{1}A$_1$ bands, respectively. That the peak maxima appear at the low-energy part of the spectrum can be explained with the fact that the minimum of the c^{1}E and b^{1}A$_1$ states is nearly co-incident with that of the electronic ground state (see Figure 4) and therefore, the initial $\phi_{00}(q_1,q_2)$ wave function overlaps greatest with the lowest vibrational levels. Specifically, the maximum overlap is achieved with the second and first vibrational levels of the c^{1}E and b^{1}A$_1$ states, respectively. Within the precision that the simulation allows (number of sampling points in the region of interest), the separation between the peaks is rather regular (ca. 400 cm^{-1}) in both bands, and corresponds to the Co−CO stretching vibration.

The theoretical spectrum of CH$_3$Co(CO)$_4$ (top of Figure 6) also presents two bands associated to the bound c^{1}E and b^{1}A$_1$ states, though the shape of the bands differs from those of HCo(CO)$_4$. The lowest energy band, extending from 42 580 to 43 800 cm^{-1} is more intense than the broader higher energy band, which appears between 50 000 and 55 000 cm^{-1}. The relative intensities are due to the different transition dipole moments as well as the amount of overlap with corresponding vibrational levels of the c^{1}E and b^{1}A$_1$ states (cf. eqs 6 and 7). The band positions are shifted with respect to the MS-CASPT2 energies (cf. Table 4); however, the qualitative structure of the peaks

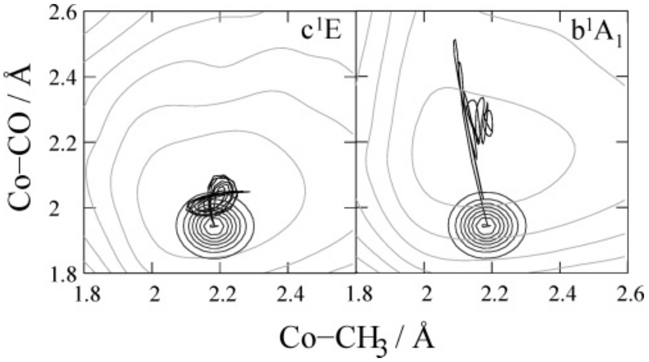

Figure 7. Contours of the initial wavefunction $\phi_{00}(q_1,q_2)$ superimposed on the c^{1}E (a) and b^{1}A$_1$ (b) 2-D potential energy surfaces along the q_1 and q_2 coordinates of CH$_3$Co(CO)$_4$. The trajectory of the center of mass of the corresponding time-dependent wave packet evolving in time have also been plotted.

should acquiesce independent of the employed method. Interestingly, the first band (peaking at 42 600 cm^{-1}) does not show regular spacing as in HCo(CO)$_4$. This is due to the overlap of the initial wave function $\phi_{00}(q_1,q_2)$ with the one propagated in time. The wave function constantly overlaps the original wave function along both degrees of freedom which over time affects the shape of the autocorrelation function. The initial wave function $\phi_{00}(q_1,q_2)$ superimposed on the c^{1}E potential along with the trajectory of the center of the wave packet evolving over 1 ps is shown in Figure 7a. As can be seen, the motion of the wave packet is focused within a small region, moving along both degrees of freedom. The irregular spacing of the first band on Figure 6 corresponds to the vibrational eigenstates on the c^{1}E PES, and indicates that the motion of the wave packet incorporates a mixture of Co−CO$_{ax}$ and Co−CH$_3$ stretching. In contrast, the motion of the wave packet in the b^{1}A$_1$ state (Figure 7b) is mostly along the Co−CO stretching coordinate in which the wave packet moves farther away from its original position. The autocorrelation function is mostly affected from this motion and therefore the second band (peaking at 52 050 cm^{-1}) shows a regular spacing of about ca. 300 cm^{-1}, corresponding to the Co−CO vibration in the b^{1}A$_1$ state (see inset of Figure 6).

4. Conclusion

The photoreactivity of RCo(CO)$_4$ (R=H, CH$_3$) has been investigated on the basis of CASSCF state correlation diagrams connecting the electronic ground state and the low-lying^{1,3}E and^{1,3}A$_1$ states as a function of the Co−R and Co−CO$_{ax}$ bond elongations and associated 2-D PES. Absorption spectra have been calculated by means of time-dependent wave packet propagations. Intense bands in the UV absorption domain, attributed to the c^{1}E and b^{1}A$_1$ MLCT excited states, characterize both complexes. The low-lying a^{1}E and b^{1}E MSBCT states as well as their triplet counterpart are dissociative with respect to both channels, namely the CO loss and the Co−R bond homolysis, whereas the ^{3}A$_1$ ($\sigma_{\text{Co−R}}$ $\sigma^*_{\text{Co−R}}$) state is bound for the carbonyl stretch. The upper MLCT states do not play any role in the photoreactivity of these molecules. The key excited states are the b^{1}E (3d$_{\text{Co}}$ → $\sigma^*_{\text{Co−R}}$) calculated at 40 280 cm^{-1} for HCo(CO)$_4$ and 38 390 cm^{-1} for CH$_3$Co(CO)$_4$, and are potentially photoactive as initiators of ultrafast, direct photofragmentation into RCo(CO)$_3$ + CO and R$^\bullet$ + $^\bullet$Co(CO)$_4$. According to wave packet simulations on CASSCF potentials in the adiabatic scheme and within the limits of the present study based on 2-D PES, both ligands dissociate in CH$_3$Co(CO)$_4$, while the homolysis is the most favorable process in HCo(CO)$_4$. This is in contrast to classical experiments performed for HCo(CO)$_4$ in low-temperature matrices under irradiation at 254 nm[5] which point to the CO loss as major process. In order to validate the present simulation, laser pump−probe experiments[26,27,28] able to detect the photofragments in a femtosecond time scale would be necessary. Further theoretical models should incorporate non-adiabatic effects and increase the nuclear dimensionality.

Acknowledgment. The PROCOPE bi-lateral program N°07579RB and the SFB 450 “Analysis and control of ultrafast photoinduced reactions” are gratefully acknowledged. The calculations have been performed either on the HP workstations of the Theoretische Chemie group at FU-Berlin or on the workstations of the LCQS (Strasbourg) and at the IDRIS national computer center (Orsay). LG thanks the “Berliner Förderprogramm” for financial support.

References and Notes

(1) Kim, S. K.; Pedersen, S.; Zewail, A. H. *Chem. Phys. Lett.* **1995**, *233*, 500.

(2) Rossenaar, B. D.; Kleverlaan, C. J.; Stufkens, D. J.; Oskam, A. *J. Chem. Soc., Chem. Commun.* **1994**, 63; Rossenaar, B. D.; Stufkens, D. J.; Oskam, A.; Fraanje, J.; Goubitz. K. *Inorg. Chim. Acta* **1996**, *247*, 215.

(3) Boese, W. T.; Ford, P. C. *Organometallics* **1994**, *13*, 3525; Horton-Mastin, A.; Poliakoff, M.; Turner, J. J. *Organometallics* **1986**, *5*, 405.

(4) Sweany, R. L. ; Russell, F. N. *Organometallics* **1988**, *7*, 719.

(5) Sweany, R. L. *Inorg. Chem*. **1982**, *21*, 752.

(6) Church, S. P. ; Poliakoff, M. ; Timney, J. A. ; Turner, J. J. *Inorg. Chem*. **1983**, *22*, 3259.

(7) Ziegler, T.; Tschinke, V.; Becke, A. *J. Am. Chem. Soc*. **1987**, *109*, 1351; Folga, E.; Ziegler, T. *J. Am. Chem. Soc*. **1993**, *115*, 5169.

(8) Jonas, V.; Thiel, W. *J. Chem. Phys*. **1996**, *105*, 3636; Goh, S. K.; Marynick, D. S. *Organometallics* **2002**, *21*, 2262.

(9) Veillard, A.; Strich, A. *J. Am. Chem. Soc*. **1988**, *110*, 3793.

(10) Daniel, C.; Heitz, M. C.; Lehr, L.; Manz, J.; Schröder, T. *J. Phys. Chem*. **1993**, *97*, 12485; Heitz, M. C.; Ribbing, C.; Daniel, C. *J. Chem. Phys*. **1997**, *106*, 1421.

(11) Daniel, C. *J. Am. Chem. Soc*. **1992**, *114*, 1625; Hachey, M. R.; Daniel, C. *Inorg. Chem.* **1998**, *37*, 1387.

(12) Ambrosek, D.; Villaume, S. ; González, L.; Daniel, C. *Chem. Phys. Lett.* **2006**, *417*, 545.

(13) McNeill, E. A.; Scholer, F. R. *J. Am. Chem. Soc*. **1977**, *99*, 6243.

(14) Siegbahn, P. E. M.; Almlöf, J.; Heiberg, A.; Roos, B. O. *J. Phys. Chem*. **1981**, *74*, 2384.

(15) Finley, J.; Malqvist, P.-A.; Roos, B. O.; Serrano-Andres, L. *Chem. Phys. Lett*. **1998**, *288*, 299.

(16) Andersson, K.; Barysz, M.; Bernhardsson, A.; Blomberg, M. R .A.; Carissan, Y.; Cooper, D. L.; Fülscher, M. P.; Gagliardi, L.; de Graaf, C.; Hess, B. A.; Karlström, G.; Lindh, R.; Malmqvist, P.-Å.; Nakajima, T.; Neogrády, P.; Olsen, J.; Roos, B. O.; Schimmelpfennig, B.; Schüz, M.; Seijo, L.; Serrano-Andrés, L.; Siegbahn, P. E. M.; Stålring, J.; Thorsteinsson, T.; Veryazov, V.; Widmark, P.-O. *MOLCAS 6.0*; Lund University: Sweden, 2004.

(17) Pierloot, K.; Dumez, B.; Widmark, P. −O.; Roos, B. O. *Theor. Chim. Acta* **1995**, *90*, 87.

(18) Heller, E. J. *Acc. Chem. Res*. **1981**, *14*, 368.

(19) Marston, C. C.; Balint-Kurti, G. G. *J. Chem. Phys*. **1989**, *91*, 3571.

(20) Feit, M. D.; Fleck, J. A.; Steiger, A. *J. Comput. Chem*. **1982**, *47*, 412.

(21) Schmidt, B. *WavePacket 4.2: A Program Package for Quantum-Mechanic Wavepacket Propagation*; Free University Berlin: Berlin, 2005.

(22) Balakrishman, N.; Kalyanaraman, C.; Sathyamurthy, N. *Phys. Rep.* **1997**, *280*, 79.

(23) Ungvary, F. *J. Organomet. Chem*. **1972**, *36*, 363.

(24) Ziegler, T.; Tschinke, V.; Becke, A. *J. Am. Chem. Soc*. **1987**, *109*, 1351.

(25) Ehlers, W. A.; Frenking, G. *Organometallics* **1995**, *14*, 423.

(26) Trushin, S. A.; Fuss, W.; Schmid, W. E.; Kompa, K. L. *J. Phys. Chem. A* **1998**, *102*, 4129.

(27) Gutmann, M.; Janello, J. M.; Dickebohm, M. S.; Grossekathöfer, M.; Lindner-Roenneke, J. *J. Phys. Chem. A* **1998**, *102*, 4138 and references therein.

(28) Daniel, C.; Full, J.; González, L.; Lupulescu, C.; Manz, J.; Merli, A.; Vajda, S.; Wöste, L. *Science* **2003**, *299*, 536.